JOURNAL OF MATERIALS SCIENCE **34** (1999) 1061–1071

Microstructure and mechanical properties of transient liquid phase bonds between NiAl and a Nickel-Base superalloy

W. F. GALE, Y. GUAN
Auburn University, Materials Research and Education Center, 201 Ross Hall, Auburn, AL 36849, U.S.A.
E-mail: wfgale@eng.auburn.edu

An investigation of microstructural development in transient liquid phase bonds between the B2 type intermetallic compound NiAl and a nickel-base superalloy MM–247 is presented in this paper. The bonds discussed in the paper employed pure copper interlayers. Based on edge-on transmission electron microscopy investigations, the paper examines both microstructural development at the bond-line and the influence of bonding on the adjacent substrates. The paper considers the epitaxial growth of the B2 type β (nominally NiAl) phase into the joint and the formation of non-epitaxial β-phase layers. The paper also examines the formation of second-phases, including the $L1_2$ type γ'-phase (nominally $Ni_3(Al, Ti)$), MX type carbides, σ-phase intermetallics and elemental chromium and tungsten.

Bond-line and adjacent substrate microstructures for the NiAl/Cu/MM–247 bonds are correlated with joint mechanical properties determined by room-temperature shear testing. The paper compares the microstructure and mechanical properties of NiAl/Cu/MM–247 bonds with those of NiAl/Cu/Ni joints.

1. Introduction

Transient liquid phase (TLP) bonding [1] provides a means of joining materials, such as the intermetallic compound NiAl, which are unsuitable for fusion welding or diffusion bonding (as a result, for example, of the formation of stable oxide layers on the faying surfaces and poor room-temperature ductility). The authors have previously demonstrated that the formation of TLP bonds between NiAl and commercially pure nickel is possible by the use of commercially pure copper interlayers [2]. Changes in the ratio of copper to nickel both with location in the joints and bonding time led to the formation of complex and evolving microstructures. The complexity and microstructural evolution of these bonds resulted from competition between:

- the stabilization of the disordered γ-phase (face centered cubic Ni–Al–Cu solid-solution) by copper [3];
- the formation of both the B2 type β-phase (nominally NiAl) and $L1_2$ type γ' (nominally Ni_3Al) intermetallics by reaction between nickel and aluminum [4].

It is also noteworthy that the TLP bonding process in NiAl/Cu/Ni bonds employed conditions somewhat different from those assumed in standard models of the TLP process [e.g. 5–8]. These models were developed for systems in which an eutectic is formed at the bond-line, either directly from a multi-component interlayer, or by reaction between the interlayer and the substrates. In contrast, the NiAl/Cu/Ni bonds formed a liquid at the bond-line by direct melting of the pure copper interlayer. Subsequent isothermal solidification proceeded as a result of gradual entry throughout the bonding process of nickel (originating from both the NiAl and nickel substrates) and aluminum (from the NiAl substrate) into the bond-line region. These compositional changes, in turn, induced an increase in the melting temperature of the liquid and hence the progression of isothermal solidification.

Despite the complexity of the NiAl/Cu/Ni bonds, these bonds were far more successful (in terms of joint microstructure) than NiAl–Ni joints employing a commercial Ni–4.5 wt % Si–3.2 wt % B interlayer (denoted by the American Welding Society as BNi–3). When the latter were investigated by one of the authors [9, 10], these bonds were found to suffer from the formation of stable borides (with a 1065 °C bonding temperature) or extensive liquation damage to the nickel substrate (with an 1150 °C bonding temperature). Also, the use of pure copper interlayers offers a lower bonding temperature (e.g. 1150 °C) than could be employed for alternative TLP bonding strategies such as the formation of NiAl by in-situ synthesis [11] or the use of nickel-rich interlayers generated in-situ during a high-temperature vacuum pre-exposure treatment [12].

An investigation is undertaken in the present paper of the extent to which the use of copper interlayers is applicable to the joining of NiAl to complex commercial nickel-base superalloys, rather than just to an NiAl/

Cu/Ni model system. Thus, the present paper examines microstructural development in copper-interlayer TLP bonds between NiAl and a "typical" nickel-base superalloy, namely, Martin-Marietta (MM) 247. The microstructures formed in NiAl/Cu/MM–247 bonds are compared and contrasted with those observed in previous work by the authors on the NiAl/Cu/Ni system [2]. The present paper also characterizes the mechanical properties of both NiAl/Cu/MM–247 and NiAl/Cu/Ni bonds in terms of room-temperature shear-strength and correlates the bond strength observations with the microstructures observed at the bond-line.

2. Experimental techniques

The materials employed for the TLP bonds were all polycrystalline and the condition of these materials prior to bonding was as follows:

- nominally stoichiometric NiAl: received in an as-cast condition and then homogenized for 48 hours at 1350 °C, resulting in a grain size of around 200 μm;
- commercial purity (99.8 wt %) copper: received in the form of wrought sheet with a thickness of 50 μm;
- MM–247 (nominally Ni–10 wt % Co–10 wt % W–8.3 wt % Cr–5.5 wt % Al–3 wt % Ta–1.5 wt % Hf–1 wt % Ti–0.7 wt % Mo–0.14 wt % C–0.05 wt % Zr–0.015 wt % B): received in a cast condition and solution treated for 4 hours at 1200 °C followed by water quenching to room temperature, resulting in a grain size of around 50 μm for the MM–247;

NiAl/Cu/MM–247 bonds were prepared using holding times of up to 12 hours at 1150 °C under a 10^{-4} Pa vacuum. A heating rate of 2 °C s^{-1} and a cooling rate of 1.5 °C s^{-1} were employed for the bonding treatments. NiAl/Cu/MM–247 samples bonded for two hours at 1150 °C were subjected to a two step post-bond ageing treatment. This treatment consisted of a primary ageing stage comprised of 30 hours holding at 950 °C, followed by air cooling to room-temperature and a secondary ageing step involving a 16 hour hold at 725 °C, followed by air cooling to room-temperature. This ageing treatment was intended to be generic to γ/γ' superalloys and was not tailored to achieving a specific γ' distribution in the MM–247 material.

The mechanical properties of NiAl/Cu/MM–247 samples bonded for two hours at 1150 °C and subjected to the full post-bond ageing treatment described above were characterized by room-temperature shear testing. For the shear tests, the procedure developed by Yan and Wallach for diffusion bonded intermetallic compounds [13] was employed. Shear tests on the NiAl/Cu/MM–247 samples were compared with results obtained for NiAl/Cu/Ni joints prepared under similar conditions.

Both as-bonded and heat treated NiAl-superalloy TLP bonds were characterized by cross-sectional transmission electron microscopy (TEM). Edge-on specimens were prepared by liquid nitrogen cold-stage ion milling, using a Gatan DuoMill operated at 5 kV with dual argon ion guns located at 13° to the sample and with currents of 500 mA per gun. Metallographic samples were prepared by electro-etching at 3 V in a solution consisting of 30 vol % acetic acid, 30 vol % lactic acid, 20 vol % hydrochloric acid, 10 vol % nitric acid and 10 vol % distilled water.

TEM was conducted using a JEOL JEM–2010 instrument operated at 200 kV. In this paper, the beam direction is denoted by "**B**" and the reciprocal lattice vector of the reflection used to form dark field ("DF") images is indicated by **g**. The following abbreviations are employed: bright field—"BF", and selected area diffraction—"SAD".

Scanning electron microscopy was employed both to characterize bond cross-sections and also for fractographic investigations. SEM employing both secondary electron (SEI) and backscattered electron (BEI) imaging was conducted using a JEOL JSM–840 instrument operated at 20 kV. Energy dispersive X-ray (EDS) analysis was conducted using Link Isis analyzers and ultra-thin window (UTW) detectors attached to the JSM-840 (operated at 20 kV) and JEM–2010 (operated at 200 kV) instruments. Quantitative, ZAF corrected SEM-based EDS analyses were performed using a probe current of approximately 1 nA on polished, but unetched metallographic cross-sections of the NiAl/Cu/MM–247 bonds. TEM-based EDS analyses were treated as qualitative.

3. Results and discussion

In this section, the microstructures and mechanical properties observed in as-bonded NiAl/Cu/MM–247 joints will be contrasted with those noted in previous work on model NiAl/Cu/Ni bonds. The influence of post-bond heat-treatment on the NiAl/Cu/MM–247 bonds will also be assessed.

3.1. Microstructural development in as-bonded and heat-treated NiAl/Cu/MM–247 TLP bonds

In this section, the overall microstructure of the NiAl/Cu/MM–247 bonds will first be compared with that of the NiAl/Cu/Ni joints. The precipitation of second phases will then be considered in detail.

3.1.1. Progression of isothermal solidification

Isothermal solidification of the NiAl/Cu/MM–247 TLP bonds (Fig. 1) was dominated by epitaxial growth of nickel-rich β (typical compositional profiles are shown in Fig. 2) from the NiAl substrate and in this respect bonds involving MM–247 resembled those observed previously in the NiAl/Cu/Ni system. In the NiAl/Cu/Ni system [2], isothermal solidification progressed relatively slowly and 6 hours holding at 1150 °C was required to fully isothermally-solidify the bonds. In contrast, isothermal solidification in the NiAl/Cu/MM–247 system was extremely rapid and was completed after only 20 minutes holding at 1150 °C. Copper

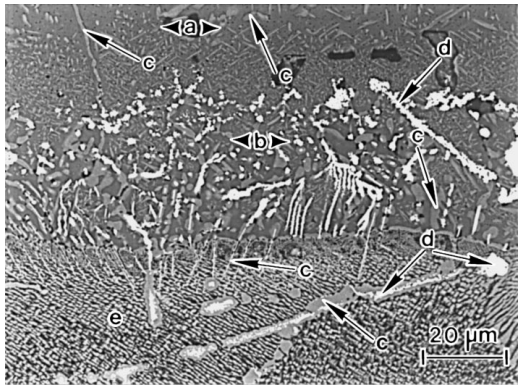

(a)

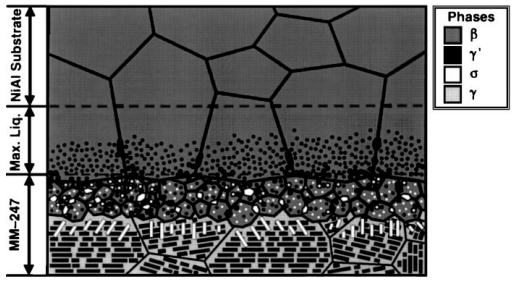

(b)

Figure 1 The overall microstructure of NiAl/Cu/MM–247 bonds: a) BEI showing a sample bonded for 2 hours at 1150 °C, followed by post-bond heat-treatment for 30 hours at 950 °C and 16 hours at 725 °C (a = region possessing a β-phase matrix epitaxial with the bulk NiAl substrate, b = region with a non-epitaxial β-phase matrix, c = γ' precipitates, d = σ-phase and e = γ/γ' matrix of the MM–247 substrate). b) Schematic showing the major microstructural features observed in the bonds ("max liq." indicates the maximum liquid width produced during bonding).

was readily dispersed within both substrates of the NiAl/Cu/MM–247 bonds as can be seen from Fig. 2. The redistribution of copper (and other elements) was such that, after only 2 hours at 1150 °C, the maximum copper content observed within the bonds (i.e. the copper content at the bond center-line) did not exceed 7 at %. In comparison the peak copper content of the NiAl/Cu/Ni bonds remained at over 30 at % after 2 hours holding at 1150 °C [2]. However, given the compositional complexity of the MM–247 alloy and the redistribution of multiple alloying elements during dissolution of the substrates and isothermal solidification, the origins of the difference in isothermal solidification rate between the NiAl/Cu/Ni and NiAl/Cu/MM–247 systems remains unclear at the present time.

3.1.2. Epitaxial and non-epitaxial growth of the β-phase

Although the isothermal solidification of the NiAl/Cu/MM–247 bonds was accomplished predominantly by epitaxial growth from the NiAl substrate, a region of the bonds in the vicinity of the nickel substrate–joint interface consisted of fine-grained polycrystalline NiAl typically with a grain size of around 5–10 μm. This region typically possessed a width of around 30 μm and may be seen in Fig. 1. In TEM investigations, the grain boundaries in the fine-grained region were found to be of the random high-angle type. Furthermore, the grain size of the fine-grained region was far smaller than that of the bulk NiAl (typically around 200 μm). Similarly, the grain boundaries of the fine-grained NiAl region showed no correspondence with those of the MM–247 substrate. Given the compositional and structural similarity between the NiAl substrate material and the ingrowing β-phase solid, the bonds would be expected to isothermally solidify by epitaxial growth. Indeed epitaxial growth is commonly observed experimentally in TLP bonds [e.g. 1, 10, 14]. Thus, the formation of a region of fresh nucleation and growth is unexpected and significant and is now discussed further.

At first sight, the fine-grained NiAl region formed in the vicinity of the MM–247 substrate of the NiAl/Cu/MM–247 joints might seem analogous to β-phase precipitates formed at the joint–nickel substrate interface of NiAl/Cu/Ni bonds [2]. However, two significant differences were observed between the β-phase deposits in the NiAl–nickel and NiAl–MM–247 bonds. These differences were as follows:

- The β-phase found at the joint–nickel substrate interface of NiAl/Cu/Ni bonds was invariably orientation related to the nickel substrate. In contrast, the β-phase formed in the NiAl/Cu/MM–247 joints bore no orientation relationship to the nickel substrate.
- The joint–nickel substrate interface region of the NiAl/Cu/Ni bonds, in which the precipitation of β-phase occurred was locally enriched in (aluminide forming) aluminum, when compared with (γ-stabilizing [3]) copper. Such a localized increase in the aluminum to copper ratio was not apparent in the fine grained β-phase region of the NiAl/Cu/MM–247 bonds.

Given these differences, it would appear that the mechanism leading to the precipitation of the β-phase in the vicinity of the nickel-base substrate–joint interface differs significantly between the NiAl/Cu/Ni and NiAl/Cu/MM–247 joints.

Diffusion induced recrystallization has been documented in TLP bonded, oxide dispersion strengthened nickel-base superalloys [15]. However, this recrystallization takes place under the influence of a high diffusional flux of mis-fitting interstitial boron out of a boron-rich interlayer into heavily cold worked substrates. Similar conditions did not exist in the present work. Hence, diffusion-induced recrystallization would not seem a plausible explanation for the formation of the fine-grained non-epitaxial region.

In searching for an alternative mechanism for the formation of the fine-grained, non-epitaxial β-phase region of the NiAl/Cu/MM–247 joints, a comparison can be drawn between this region and pack aluminide diffusion coatings on nickel-base superalloys. These coatings [16–19] are produced by aluminum enrichment of the surface of a superalloy by contact with an aluminum-containing vapor phase. The near-surface region of the superalloy is transformed to the β-phase during coating and an additional diffusion

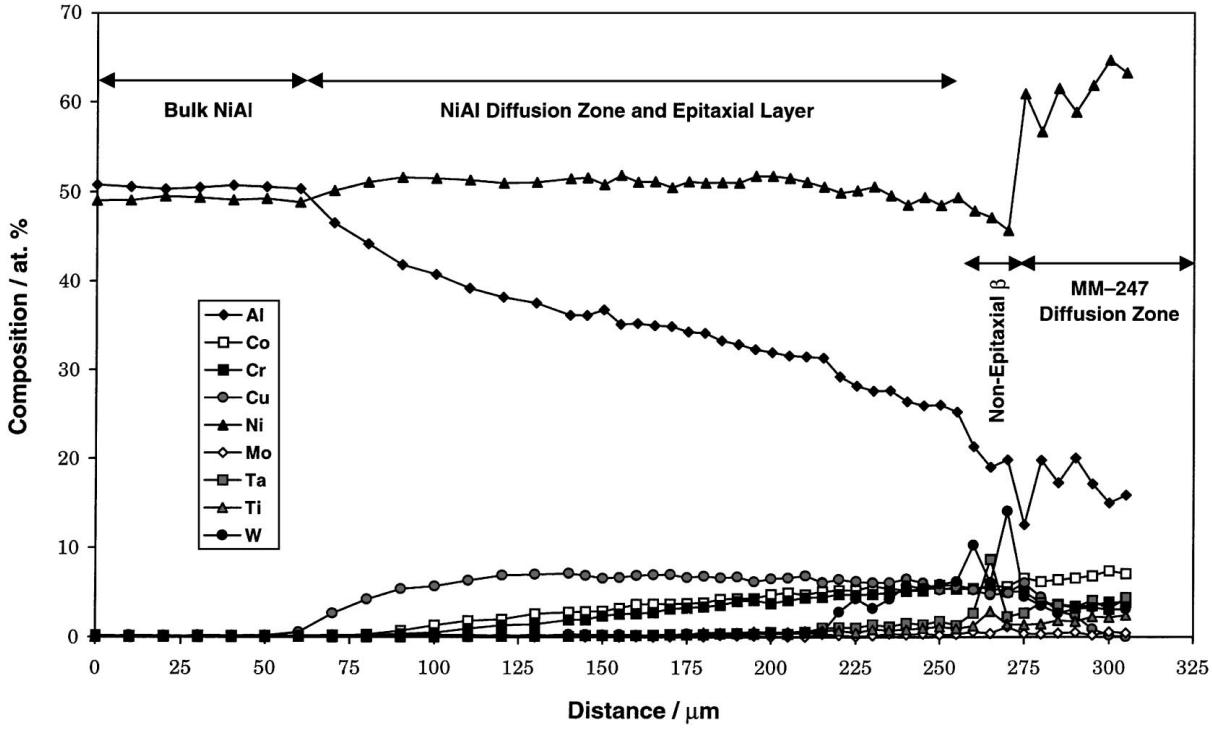

(a)

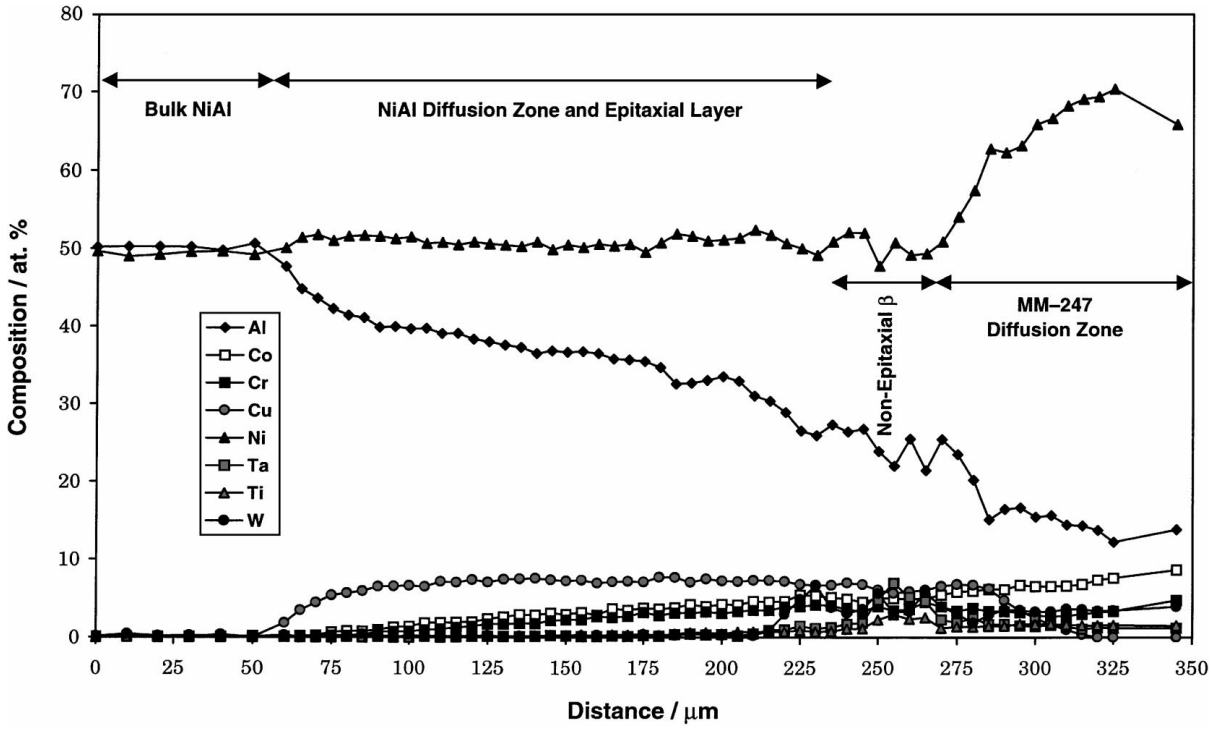

(b)

Figure 2 SEM-derived EDS compositional profiles for NiAl/Cu/MM–247 joints: a) As-bonded for 2 hours at 1150 °C. b) Bonded for 2 hours at 1150 °C, followed by post-bond heat-treatment for 30 hours at 950 °C and 16 hours at 725 °C.

treatment [16–19]. The actual formation of the β-phase takes place *entirely in the solid state*. Depending on the compositional and process conditions employed, formation of the coating can occur predominantly by either the diffusion of aluminum (i.e. from the surface into the bulk superalloy) or the outward diffusion of nickel [20]. In either case, a random polycrystalline coating is invariably produced, even on a single-crystal superalloy substrate, and so an orientation relationship is not observed between the β-phase coating matrix and the superalloy's γ-phase matrix [21].

Based on the description of aluminide diffusion coatings given above, a possible process for the formation of the polycrystalline β-phase layer in the NiAl/Cu/MM–247 TLP bonds can be formulated. In this process, a portion of the MM–247 substrate immediately adjacent to the joint is transformed in the solid-state to the β-phase. Such a transformation would be induced

by the diffusion of aluminum (originally transferred to the joint region from the NiAl substrate) from the joint into the superalloy substrate, during and/or immediately after isothermal solidification. In such a case, the polycrystalline β-layer would be located on the substrate side of the substrate–joint interface. Indeed, experimentally, the polycrystalline layer was found to be located in a region originally contained within the MM–247 substrate (although it should be cautioned that localized dissolution of the MM–247 substrate would have moved the location of the solid-liquid interface somewhat*). Furthermore, support for the suggestion that the polycrystalline region was formed by transformation of the MM–247 substrate was obtained from observations of the nature of second phase precipitates found in this region, as will be discussed in subsequent sections.

Once isothermal solidification was completed (after 20 minutes holding at 1150 °C), the microstructure of the β-phase matrix of the NiAl/Cu/MM–247 joints was little changed either after further holding at 1150 °C or by post-bond heat treatment at 950 and 725 °C. In contrast, the precipitation of second phases was significantly modified by thermal exposure after the completion of isothermal solidification.

3.1.3. Precipitation of α-phases

Within the region of the joint that resolidified by epitaxial growth of the β-phase from the NiAl substrate, the precipitation of a disordered body centered cubic second phase (commonly denoted as "α") with a lattice parameter similar to that of the β-phase was observed in samples held for 20 minutes and longer at 1150 °C. The extent of precipitation increased significantly with further holding at 1150 °C, but was not markedly enhanced by additional post-bond heat-treatment at 950 and 725 °C. Intragranularly, the α-phase formed as spheres, typically with diameters of 10 nm or less. Precipitation of the α-phase occurred preferentially on β–β grain boundaries in the form of either plates (in regions close to the MM–247 substrate) or as spheres (in regions far from the MM–247 substrate). In all cases, a cube-cube orientation relationship was observed between the α and β-phases. When the α-phase precipitated on high angle β–β boundaries, all of the α-precipitates along a given boundary (Fig. 3) established a cube–cube orientation relationship to the same β grain.

In the NiAl/Cu/MM–247 bonds, significant transfer of both chromium and tungsten occurred from the MM–247 to the bond-line β-phase. Both of these elements have a low solid-solubility in the β-phase (for example the chromium solubility in binary NiAl at a temperature of 850 °C is 4 at % [23]). Hence, it is unsurprising that the α-phase was made up of chromium and tungsten. Of these two elements, tungsten predominated in some of the α-precipitates and chromium in others. A few α precipitates were also observed to contain significant tantalum.

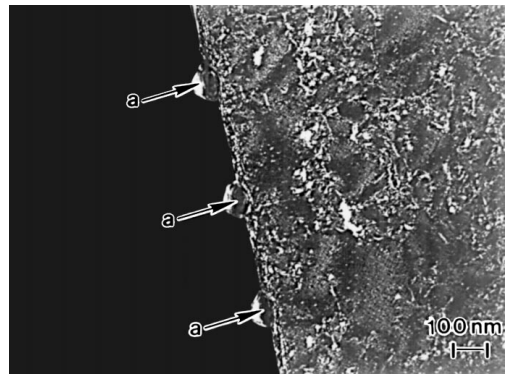

Figure 3 High angle β–β grain boundary with α precipitates. DF micrograph with $\mathbf{g} = (110)_{\beta/\alpha}$ for the right hand β grain. Notice that all three α precipitates (labeled as "a") are in contrast. This figure is taken from the portion of the joint containing β epitaxial with the NiAl substrate of NiAl/Cu/MM–247 bonded for 2 hours at 1150 °C and post-bond heat-treated for 30 hours at 950 °C.

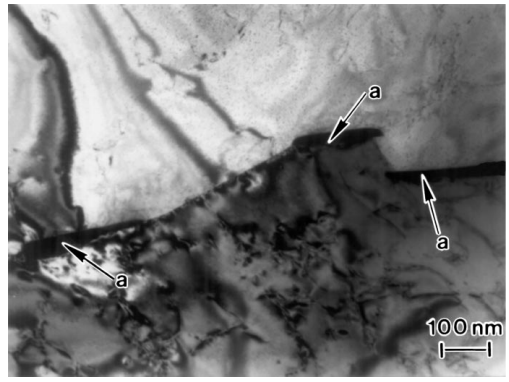

Figure 4 BF micrograph of a β–β grain boundary pinned by α-precipitates (labeled as "a"). This figure is taken from the portion of the joint containing β epitaxial with the NiAl substrate of NiAl/Cu/MM–247 bonded for 2 hours at 1150 °C and post-bond heat-treated for 30 hours at 950 °C.

A noticeable observation was that the α precipitates on β–β grain boundaries pinned these boundaries (Fig. 4), clearly indicating that the α-phase was present at a time of significant β grain growth. Furthermore, the extent to which the β grain boundaries were distorted by pinning appeared to increase somewhat with holding time at 1150 °C. Thus, it might appear that at least some of the α was precipitated at the 1150 °C bonding temperature, rather than just on cooling.

3.1.4. Formation of MX precipitates

The precipitation of face centered cubic second phases with a lattice parameter of around 430 pm was observed within the polycrystalline, non-epitaxial β-phase region present near the interface between the MM–247 substrate and the joint. These precipitates (Fig. 5) were crystallographically consistent with an MX type phase and (qualitative) TEM-based EDS assigned "M" as

* The possibility of using fixed joint gap samples (which employ spacers to define a constant joint cavity together with an applied load to extrude out of the joint cavity any excess liquid volume produced by dissolution of the substrates) was considered. However, the applied load necessary to maintain a fixed joint gap during dissolution tends to indent (e.g. tungsten) spacers into NiAl substrates when using an 1150 °C bonding temperature. Furthermore, the character of fixed and variable gap TLP bonds [22] involving NiAl differ markedly. Hence, the use of fixed joint gaps was not pursued in the present work.

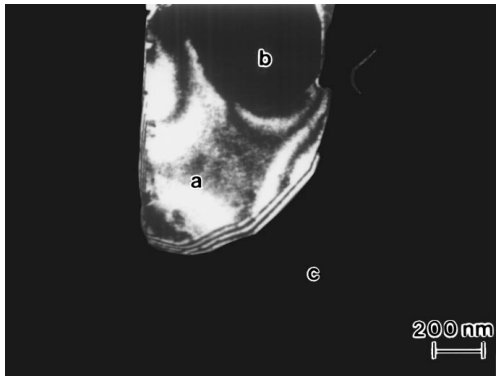

(a)

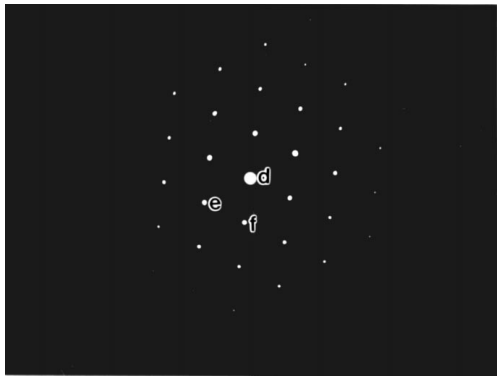

(b)

Figure 5 MX precipitates coated by γ', observed in the polycrystalline non-epitaxial β-phase region of NiAl/Cu/MM–247 bonds: a) DF image with $\mathbf{g} = (200)_{\gamma'}$ showing γ' (labeled as "a") precipitated on MX (labeled as "b") in a β-phase matrix (labeled as "c"). Bond held for 2 hours at 1150 °C. b) SAD pattern with $\mathbf{B} = [110]_{MX}$ (d = transmitted beam, e = $(002)_{MX}$ and f = $(1\bar{1}1)_{MX}$). Bond held for 2 hours at 1150 °C, followed by 30 hours at 950 °C and 16 hours at 725 °C.

titanium and "X" as carbon (a small number of hafnium and carbon rich MX precipitates were also observed). These MX precipitates were globular and typically possessed diameters of around 100 nm–1 μm. The MX precipitates did not exhibit an orientation relationship with respect to other phases present in the NiAl/Cu/MM–247 system. MX precipitation was not observed within the region of the joint that grew epitaxially from the NiAl substrate. However, MX precipitates similar to those observed within the fine grained β-phase layer were found within the bulk MM–247 substrate. The number and distribution of MX precipitates within the fine-grained (non-epitaxial) β-phase layer appeared to remain roughly constant regardless of the bonding or post-bond heat-treatment conditions employed.

Given the nature of the MX precipitation discussed above, the following points can be raised:

- Solid-state precipitation of the MX within the equiaxed β-phase layer would have been expected to result in a β–MX orientation relationship. However, such an orientation relationship was not observed experimentally.
- MX precipitates transferred from the MM–247 substrate to the liquid phase would (if not resolutioned in the liquid) tend to clump, as is observed for example in TLP bonded or brazed dispersion strengthened materials [15, 24]. On the contrary, in practice, the distribution of MX precipitates remained apparently random and similar to that in the MM–247 substrate.
- The presence of MX precipitates in the equiaxed β-phase layer, closely resembling those found in the bulk MM–247 substrate, is entirely consistent with the incorporation of pre-existing MX into the β-phase, on solid-state transformation of the superalloy substrate's γ/γ' matrix to β. This type of incorporation process is commonly observed for carbides, during the formation of aluminide diffusion coatings on nickel-base superalloys [e.g. 25].

Thus, the observed character of the MX precipitates would seem to support the formation of the fine grained, non-epitaxial β-phase layer by solid-state transformation of the MM–247 substrate.

3.1.5. Formation of σ-phase deposits

A primitive tetragonal σ-type phase (with lattice parameters a = 890 pm and c = 459 pm) was observed to form within both the equiaxed, non-epitaxial β-phase and within a localized region of the adjacent MM–247 substrate. In both cases, the σ-phase precipitates were found in (qualitative) TEM-based EDS investigations to be rich in chromium, tungsten, molybdenum, cobalt and nickel.

In the case of the σ-phase precipitated within the equiaxed, non-epitaxial β-phase, the σ (Fig. 6) was found, when precipitated intragranularly, to be polygonal (or in certain cases somewhat globular) and to typically posses a diameter of around 200 nm (although a wide range of precipitate size was observed). Extensive deposits of σ along β–β grain boundaries were also observed. The following approximate orientation relationship (Fig. 7) was noted between the β and σ-phases.

$$[\mathbf{1\,1\,1}]_\beta \;//\; [\mathbf{0\,\bar{1}\,1}]_\sigma$$
$$(\mathbf{\bar{1}\,1\,0})_\beta \;//\; (\mathbf{4\,\bar{1}\,\bar{1}})_\sigma$$

The σ-phase precipitated within the MM–247 substrate was generally in the shape of irregularly shaped needles (Figs 1 and 8). Typically, the σ needles possessed

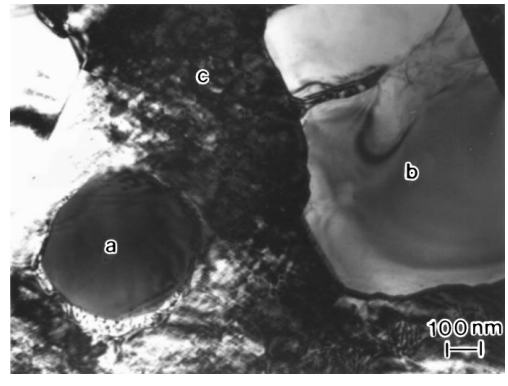

Figure 6 BF micrograph of σ and γ' precipitated in the non-epitaxial β-phase region of an NiAl/Cu/MM–247 joint held at 1150 °C for 2 hours (a = σ-phase, b = γ' and c = β).

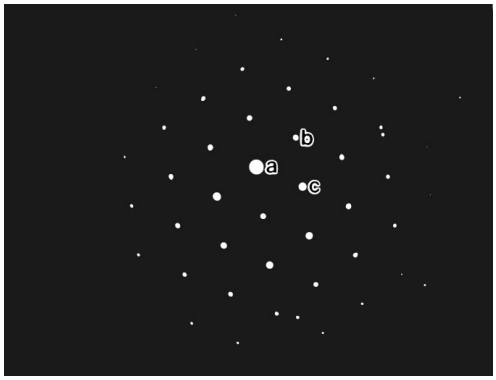

(a)

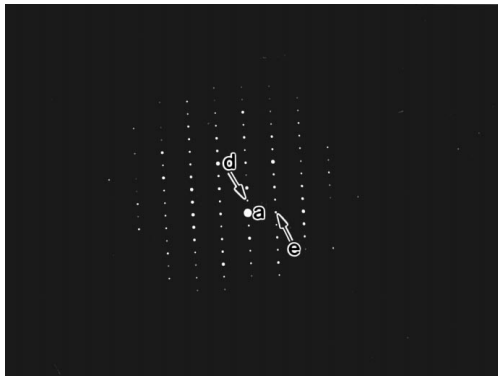

(b)

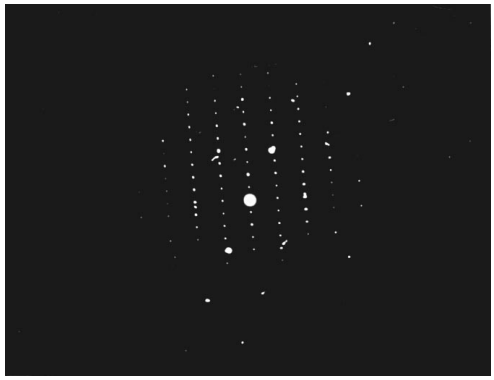

(c)

Figure 7 SAD patterns showing the crystallography of σ-phase deposits in the non-epitaxial β-phase region of NiAl/Cu/MM–247 bonded for 2 hours at 1150 °C and post-bond heat-treated for 30 hours at 950 °C (a = transmitted beam, b = $(\bar{1}10)_\beta$, c = $(01\bar{1})_\beta$, d = $(100)_\sigma$ and e = $(0\bar{1}1)_\sigma$. a) $\mathbf{B} = [111]_\beta$ showing the β-phase matrix. b) $\mathbf{B} = [0\bar{1}1]_\sigma$ showing a σ-phase precipitate. c) $\mathbf{B} = [111]_\beta \,//\, [0\bar{1}1]_\sigma$ showing the σ-precipitate to β-matrix interface.

lengths of around 1 μm and widths of around 100 nm, although σ needles extending up to around 20–40 μm in length and 4 μm in width were observed. The σ-phase needles were orientation related to the γ/γ' matrix of the superalloy as follows (Fig. 9):

$$[\mathbf{1\,1\,2}]_{\gamma/\gamma'} \,//\, [\mathbf{1\,1\,0}]_\sigma$$
$$(\bar{\mathbf{1}}\,\mathbf{1}\,\mathbf{0})_{\gamma/\gamma'} \,//\, (\mathbf{1}\,\bar{\mathbf{1}}\,\mathbf{0})_\sigma$$

The formation of σ-phase precipitates within both the equiaxed, non-epitaxial β-phase and within a localized region of the adjacent superalloy substrate is familiar from aluminide diffusion coated superalloys [e.g. 25].

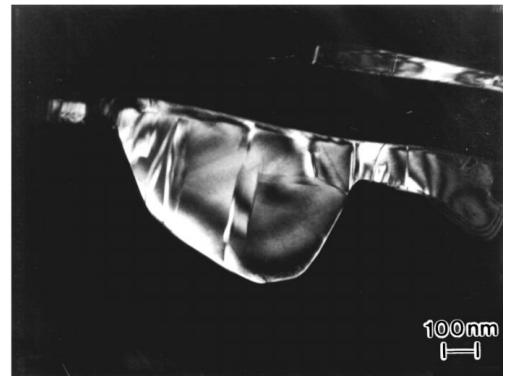

Figure 8 σ-phase precipitated in the MM–247 substrate adjacent to an NiAl/Cu/MM–247 bond held for 2 hours at 1150 °C, followed by 30 hours at 950 °C. DF micrograph with $\mathbf{g} = (001)_\sigma$ such that σ appears bright and the surrounding γ' dark.

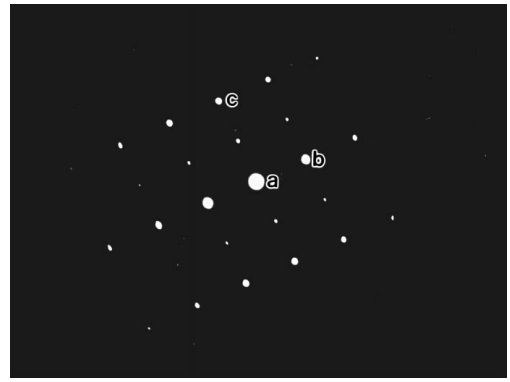

(a)

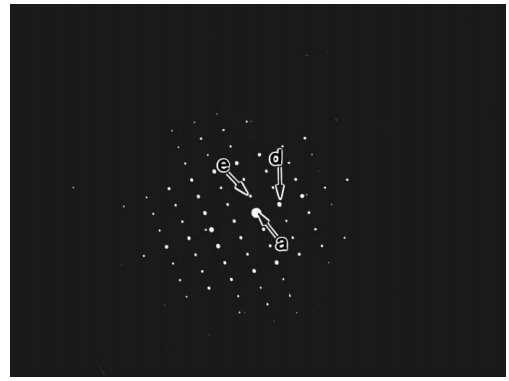

(b)

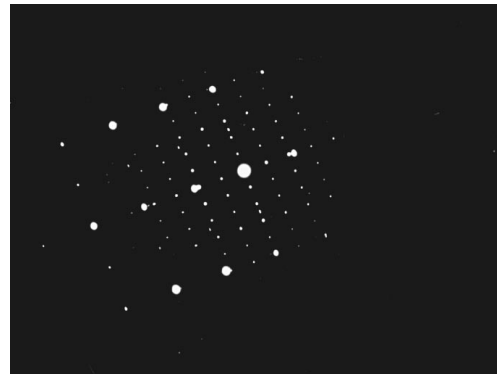

(c)

Figure 9 Crystallography of σ precipitates in the MM–247 substrate adjacent to an NiAl/Cu/MM–247 bond held for 2 hours at 1150 °C, followed by 30 hours at 950 °C (a = transmitted beam, b = $(11\bar{1})_{\gamma'}$, c = $(\bar{2}20)_{\gamma'}$, d = $(001)_\sigma$, and e = $(110)_\sigma$: a) $\mathbf{B} = [112]_{\gamma'}$ showing the γ' layer surrounding the σ-phase. b) $\mathbf{B} = [110]_\sigma$ showing the σ-phase. c) $\mathbf{B} = [112]_{\gamma'}$, $//[110]_\sigma$ showing the σ to γ' interface.

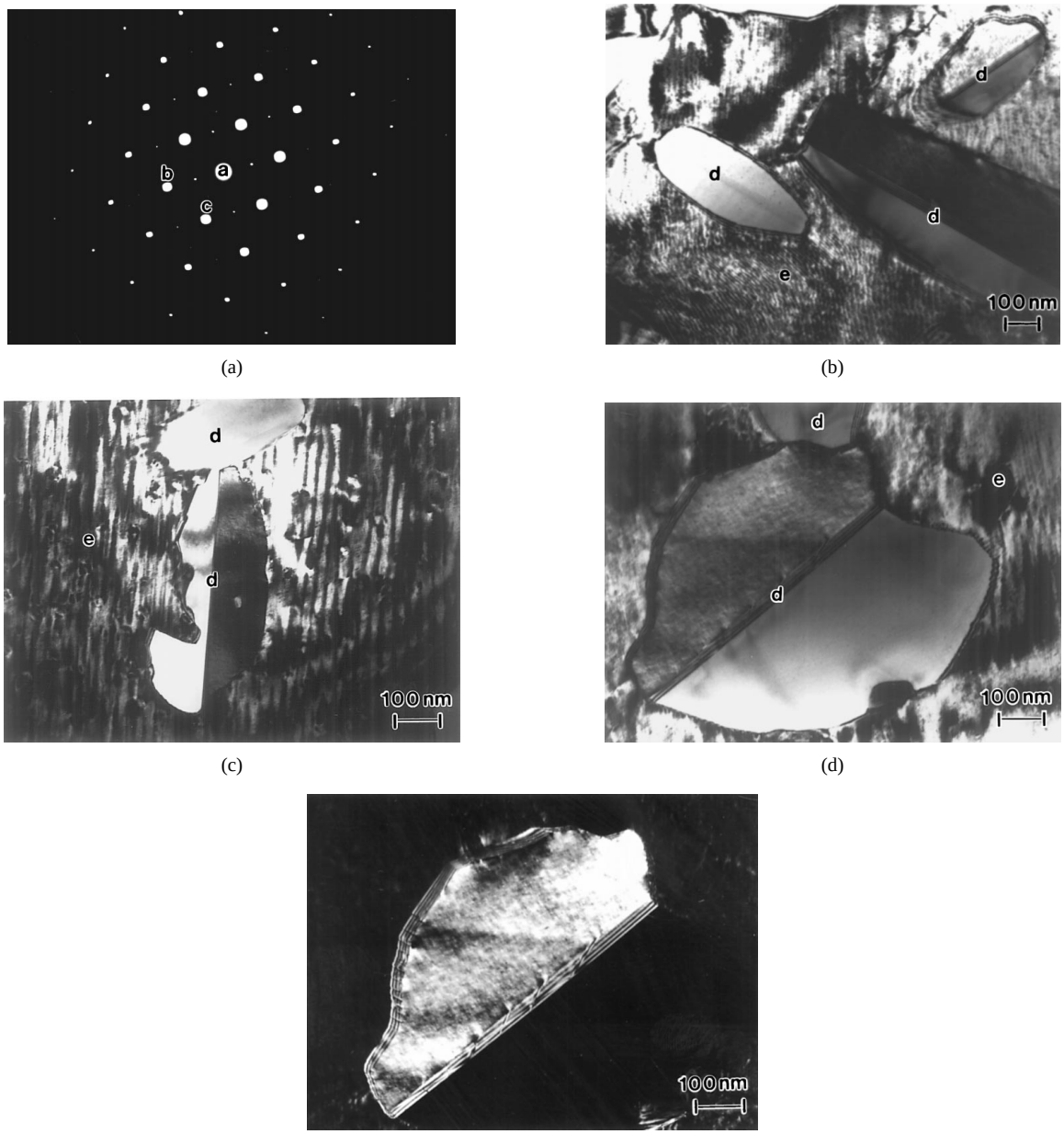

(a) (b) (c) (d) (e)

Figure 10 γ' precipitates observed in NiAl/Cu/MM–247 bonds (a = transmitted beam, b = $(002)_{\gamma'}$, c = $(1\bar{1}1)_{\gamma'}$, d = γ' and e = β): a) SAD pattern with $\mathbf{B} = [110]_{\gamma}$, identifying the γ'-phase. Sample held for 2 hours at 1150 °C, followed by 30 hours at 950 °C and 16 hours at 725 °C. b) Ellipsoidal twinned γ' precipitates imaged in BF. Sample held for 2 hours at 1150 °C, followed by 30 hours at 950 °C. c) Irregular twinned γ' morphology imaged in BF. Sample held for 2 hours at 1150 °C, followed by 30 hours at 950 °C and 16 hours at 725 °C. d) Heart-shaped twinned γ' morphology imaged in BF. Sample held for 2 hours at 1150 °C, followed by 30 hours at 950 °C. e) DF image, prepared using $\mathbf{g} = (002)_{\gamma' - 1^{st}\,\text{twin variant}}$, of the precipitate shown in Fig. 10d.

During the formation of a diffusion coating, alloying elements present in the superalloy are incorporated in the coating, and chromium, molybdenum and tungsten are subsequently precipitated out, generally as σ-phases and/or carbides [16, 25]. In the present case of NiAl/Cu/MM–247 TLP bonds, it was noticeable that the precipitation of σ within the β-phase occurred only in the fine grained, non-equiaxed region and not in β grown epitaxially from the NiAl substrate. If the fine-grained non-epitaxial region was indeed formed by solid-state transformation of a portion of the MM–247 substrate, then second-phase precipitation behavior similar to that of an aluminide diffusion coating formed under analogous circumstances might reasonably be expected. Thus the observation of extensive σ-phase formation within the fine-grained non-epitaxial region is consistent with (although not, of course, directly supportive of) formation of the fine-grained, non-epitaxial β-phase region by solid-state transformation of a portion of the MM–247 substrate.

Interdiffusion during and after the formation of aluminide diffusion coatings generally results in a significant disturbance in the composition of the superalloy substrate immediately adjacent to the coating. This disturbance is such that σ-phase (and/or extensive carbide formation) can be observed adjacent to the coating on a normally non-σ-sensitive superalloy [e.g. 25]. Presumably, the σ-phase needles observed in the MM 247 substrate immediately adjacent to the bond-line formed under similar circumstances.

3.1.6. Precipitation of γ'

The presence of γ' precipitates (Fig. 10) within the epitaxially ingrown and fine-grained non-epitaxial β-phase was a marked feature of NiAl/Cu/MM–247 bonds held for 1 hour or longer at 1150 °C. Both the 950 and 725 °C stages of the post-bond heat treatment applied to the NiAl/Cu/MM–247 bonds were found to greatly enhance the extent of this γ' precipitation. In qualitative TEM-based EDS analyses the γ' was found to consist mostly of nickel and aluminum with some titanium. Orientation relationships of the Kurdjumov–Sachs type:

$$[\mathbf{1\,1\,1}]_\beta \;//\; [\mathbf{1\,1\,0}]_{\gamma'}$$
$$(\bar{\mathbf{1}}\,\mathbf{1\,0})_\beta \;//\; (\mathbf{1}\,\bar{\mathbf{1}}\,\bar{\mathbf{1}})_{\gamma'}$$

were observed (Fig. 11) between the β and γ' phases. When precipitated directly from the β-phase, intragranular γ' precipitates were generally, but not invariably (Fig. 6), observed to form with a central midrib twin plane (Fig. 10). Twinning in γ' precipitated from nickel-rich β has been documented previously and is discussed elsewhere [26–28]. The twinned precipitates were generally roughly ellipsoidal or heart-shaped with lengths of around 100 to 500 nm and widths of around 50 to 200 nm. However, irregularly shaped and blocky intragranular γ' precipitates were also observed. Extensive precipitation of γ' was also observed along β–β grain boundaries.

Extensive precipitation of γ' (generally in the form of either plates, needles or twinned ellipsoids) was observed at the interface between the finegrained, non-epitaxial β-phase and the γ/γ' MM–247 substrate. As with the γ' formed within the joint center-line, these γ' ellipsoids were Kurdjumov–Sachs orientation related to the non-epitaxial β-phase. On the β-phase side of the β–γ/γ interface an almost continuous layer of single phase γ' was formed (Fig. 1). The growth of γ' needles from locations in the vicinity of this layer into the γ/γ' MM–247 substrate was also observed (as can be seen in Fig. 1). Given that these needles were orientation related to the β-phase (and that no orientation relationship existed between the β-phase and the γ/γ'), no orientation relationship was observed between the γ' needles and the two phase γ/γ' matrix of the MM–247 substrate.

Single-phase layers of γ' with a thickness of up to around 1–2 μm were observed to surround the σ-phase needles formed in the MM–247 substrate adjacent to the joint. Typically, the larger the σ-phase precipitate, the thicker the single phase γ' layer (such a layer is clearly visible in Fig. 1). The single-phase γ' layer surrounding the σ-needles was cube–cube orientation related to the γ/γ' matrix of the MM–247 substrate.

The appearance of a layer of near single phase γ' at the interface between the β-phase and the γ/γ' MM–247 substrate is unsurprising. However, the formation of a single-phase γ' layer around the σ-phase merits further comment. The σ-phase was found (in qualitative TEM based EDS analyses) to be aluminum-free and an aluminum-enriched region was noted around the σ-phase. Presumably the aluminum-enriched region formed as a result of rejection of aluminum from the growing σ-phase back into the surrounding matrix. This aluminum-enrichment in turn correlated with the formation of single phase γ' layers around the σ-phase precipitates.

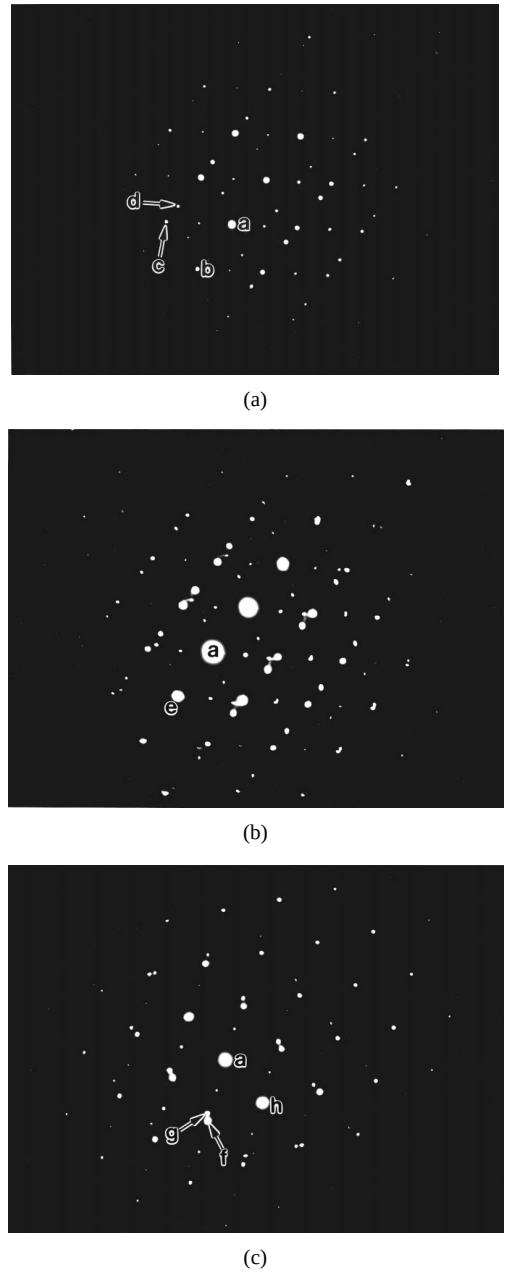

Figure 11 SAD patterns illustrating the crystallography of the γ'-phase precipitated in the β-phase matrix of NiAl/Cu/MM–247 joints. The figure shows samples held for 2 hours at 1150 °C, followed by 30 hours at 950 °C and 16 hours at 725 °C (a = transmitted beam, b = $(\bar{1}11)_{\gamma'-\text{common reflection}}$, c = $(002)_{\gamma'-1^{\text{st}}\text{ twin variant}}$, d = $(\bar{1}\bar{1}\bar{1})_{\gamma'-2^{\text{nd}}\text{ twin variant}}$, e = $(\bar{1}11)_{\gamma'}$ common with $(1\,\bar{1}\,0)_\beta$, f = $(002)_{\gamma'}$, g = $(\bar{1}10)_\beta$ and h = $(\bar{1}11)_{\gamma'}$ common with $(1\,0\,\bar{1})_\beta$): a) Twinned γ' precipitate, $\mathbf{B} = [110]_{\gamma'}$. b) Interface between the precipitate shown in figure 10a and the β-phase matrix, $\mathbf{B} = [110]_{\gamma'} \,//\, [111]_\beta$. c) Non-twinned γ' precipitate and adjacent β-phase matrix with $\mathbf{B} = [110]_{\gamma'} // [111]_\beta$.

3.2. Mechanical Properties

Significant differences in bond-line microstructure were apparent between the present work and the NiAl/Cu/Ni bonds examined previously [2]. Nonetheless,

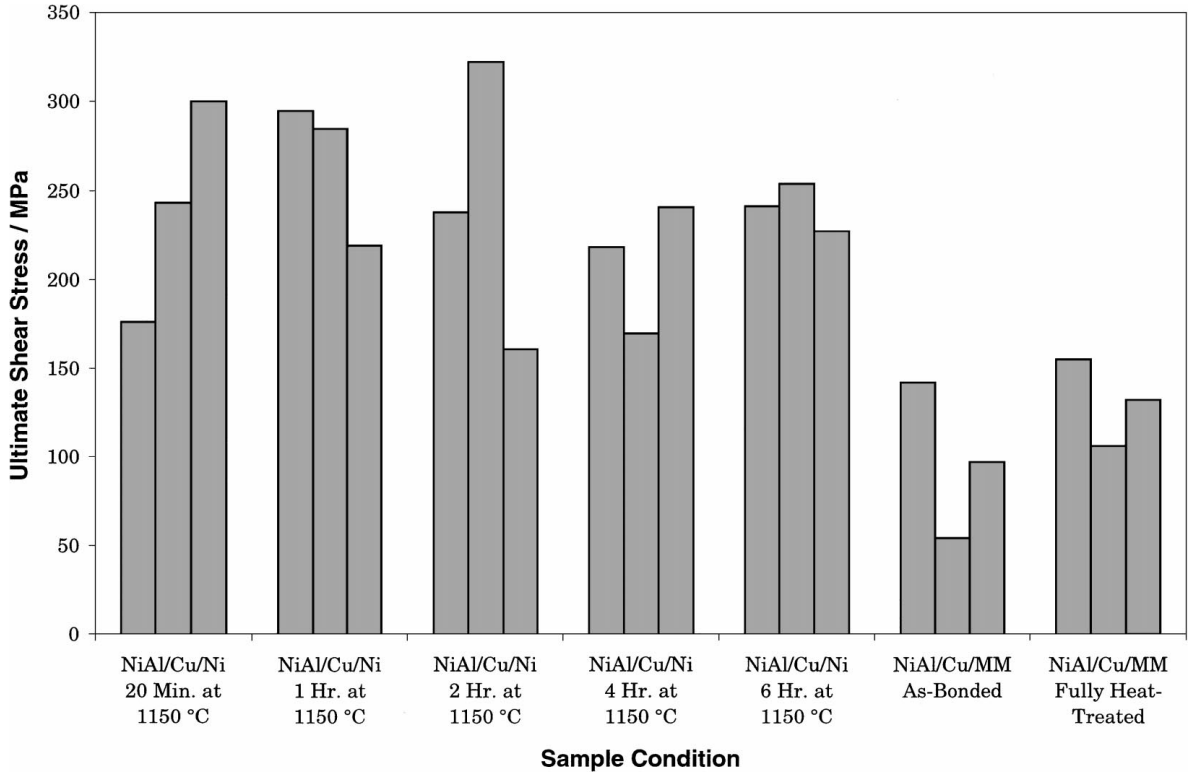

(a)

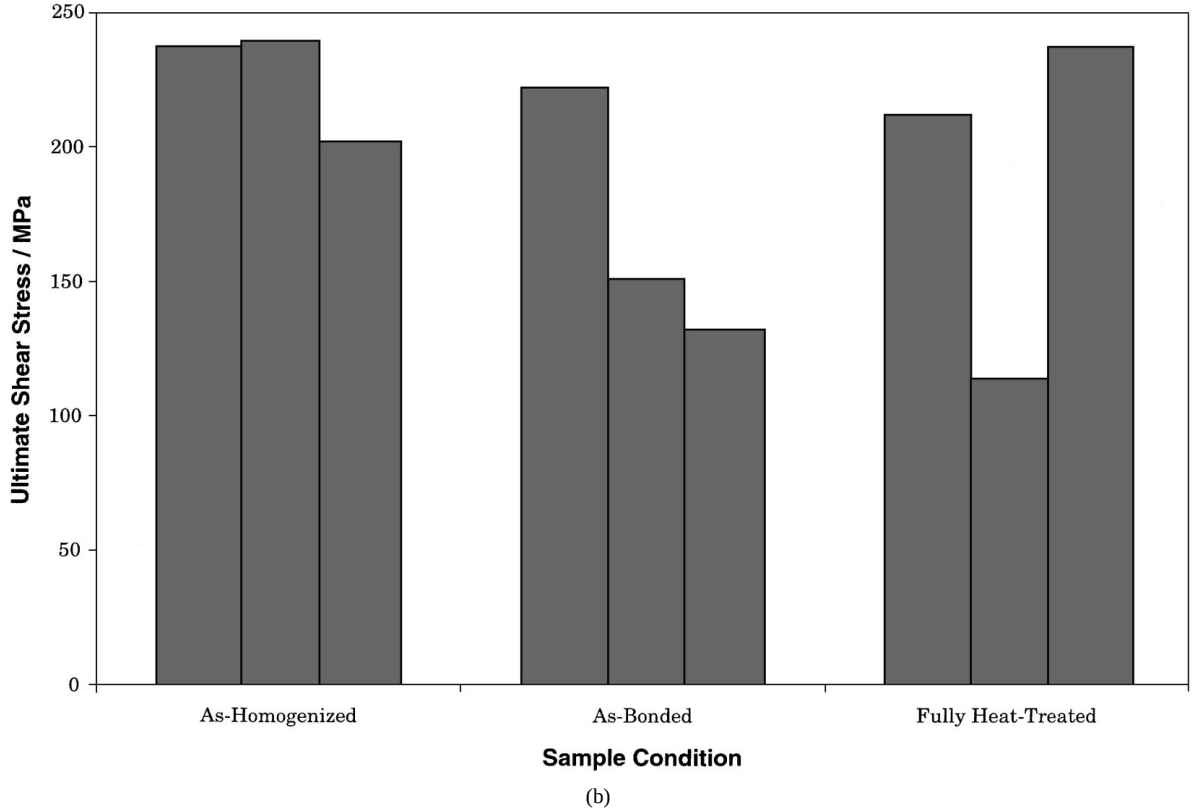

(b)

Figure 12 Shear tests conducted on NiAl/Cu/Ni and NiAl/Cu/MM–247 TLP bonds ("as-homogenized" represents the condition of the NiAl substrate prior to bonding, "as-bonded" indicates 2 hours exposure at 1150 °C and "fully heat-treated" indicates an additional 30 hours at 950 °C, followed by 16 hours at 725 °C): a) Ultimate shear stress of bonds. b) Ultimate shear stress of bulk NiAl. c) Representative fracture surface showing failure by cleavage of the bulk NiAl substrate (NiAl/Cu/Ni bond held for 20 minutes at 1150 °C). (*Continued*).

all of the shear-test samples for both the NiAl/Cu/Ni and NiAl/Cu/MM–247 bonds (Fig. 12) failed by brittle fracture of the bulk NiAl substrate. Significant scatter was observed in the shear test results, both for the bonds and the bulk NiAl substrate material (Fig. 12). However, it appeared in general that the NiAl/Cu/Ni bonds were at least comparable in strength with the bulk NiAl material, whereas the NiAl/Cu/MM–247 bonds were somewhat weaker than the bulk NiAl. The process leading to the latter observation remains unclear at the

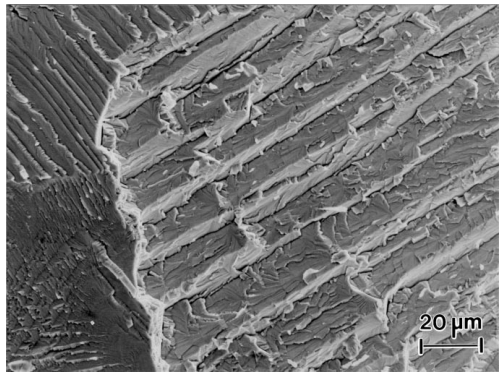

(c)

Figure 12 (*Continued*).

present time. Further investigation of factors such as compositional modification of the bulk NiAl substrate below the detection limit of EDS analysis is required.

4. Conclusions

An investigation of transient liquid phase bonding of NiAl to MM–247 using pure copper interlayers has been presented. As a result of this investigation, the following conclusions have been drawn:

- NiAl/Cu/MM–247 bonds were fully isothermally solidified after 20 minutes at 1150 °C by epitaxial growth of nickel-rich β-phase from the NiAl substrate. However, a layer of fine-grained β-phase that was non-epitaxial with the NiAl substrate was also present within the bonds. Solid state transformation of the MM–247 substrate induced by aluminum diffusion, via the joint, from the NiAl substrate has been proposed as the mechanism leading to the formation of the non-epitaxial β-phase layer. The nickel-rich β-phase formed within the joint region of NiAl/Cu/MM–247 bonds contained extensive γ' deposits. Growth of γ' into the MM–247 substrate was also noted.
- The entry of chromium and tungsten from the MM–247 substrates into the joint region correlated with the precipitation of α–(W, Cr) within the portion of the joint center-line β-phase that grew epitaxially from the NiAl substrate of NiAl/Cu/MM–247 bonds. In contrast, the non-epitaxial β-phase region of the NiAl/Cu/MM–247 bonds contained extensive inter and intragranular σ-phase deposits. Precipitation of σ-phase deposits also occurred within the MM–247 substrate immediately adjacent to the bond-line.
- Both NiAl/Cu/Ni and NiAl/Cu/MM–247 bonds failed in the NiAl substrate, rather than at the bond line. However, only the NiAl/Cu/Ni bonds exhibited shear strengths generally comparable with those of bulk NiAl.

Acknowledgements

The research described in this paper was supported by the NSF Division of Materials Research. Funding for instrumentation was provided by the NSF ARI program. The authors wish to thank Dr. E. P. George of the Oak Ridge National Laboratory and Dr. R. A. Overfelt of the Space Power Institute, Auburn University for the provision of materials used in this work.

References

1. D. S. DUVALL, W. A. OWCZARSKI and D. F. PAULONIS, *Weld. J.* **53** (1974) 203.
2. W. F. GALE and Y. GUAN, *Metall. Mater. Trans. A*, **27** (1996) 3621.
3. C. C. JIA, K. ISHIDA and T. NISHIZAWA, *Metall. Mater. Trans. A* **25** (1994) 473.
4. T. B. MASSALSKI, (ed.) "Binary Alloy Phase Diagrams," Volume II, (ASM, 1986).
5. Y. ZHOU, W. F. GALE and T. H. NORTH, *Int. Mater. Rev.*, **40** (1995) 181.
6. Y. NAKAO, K. NISHIMOTO, K. SHINOZAKI and C. Y. KANG, "Transient Liquid Insert Metal Diffusion Bonding of Ni-Base Cast Superalloy MM007," *IIW Document 1A-334-86-OE, International Institute for Welding*, 1989.
7. Y. NAKAO, K. NISHIMOTO, K. SHINOZAKI and C. Y. KANG, in *Advanced Joining Technologies*, ed. T. H. North (Chapman & Hall, 1990) pp. 129–144.
8. I. TUAH-POKU, M. DOLLAR and T. B. MASSALSKI, *Metall. Trans. A*, **19** (1988) 575.
9. W. F. GALE and S. V. OREL, *Metall. Mater. Trans. A* **27** (1996) 1925.
10. W. F. GALE and S. V. OREL, *J. Mater. Sci.* **31** (1996) 345.
11. M. J. STRUM and H. A. HENSHALL, in *Proc. Advanced Joining Technologies for New Materials II, March 2–4, 1994, Cocoa Beach, Florida*, eds. N. F. Flore and J. O. Stiegler, (AWS, Miami, FL, 1994) pp. 76–88.
12. T. J. MOORE and J. M. KALINOWSKI, *MRS Symp. Proc.*, **288** (1993) 1173.
13. P. YAN and E. R. WALLACH, *Intermetallics* **1** (1993) 83.
14. W. F. GALE and E. R. WALLACH, *Mater. Sci. Technol.* **7** (1991) 1143.
15. A. MARKHAM, *Ph.D. Thesis*, University of Cambridge, U.K., 1988.
16. J. H. WOOD and E. GOLDMAN, in "Superalloys II," eds. C. T. Sims, N. S. Stoloff and W. C. Hage (John Wiley & Sons, 1987) pp. 329–384.
17. T. N. RHYS-JONES, in "Materials Development in Turbo-Machinery Design," eds. D. M. R. Taplin, J. F. Knott and M. H. Lewis, (Institute of Metals, London, UK; Parsons Press, Dublin, Ireland, 1989) pp. 218–223.
18. T.N. RHYS-JONES and D. F. BETTRIDGE, in *Advanced Materials and Processing Techniques for Structural Applications* eds. T. Khan and A. Lasalmonie (Office National D'Etudes et de Recherches Aerospatiales, Chatillon, France, 1988) pp. 129-158.
19. T. N. RHYS-JONES, *Mater. Sci. Technol.* **4** (1988) 421.
20. S. R. LEVINE and R. M. CAVES, *J. Electrochem. Soc.* **121** (1974) 1051.
21. W. F. GALE and J. E. KING, *Metall. Trans. A* **23** (1992) 2657.
22. S. V. OREL, L. PAROUS and W. F. GALE, *Weld. J. (Res. Suppl.)* **74** (1995) 319s.
23. G. PETZOW and G. EFFENBERG (eds.) "Ternary Alloys, A Comprehensive Compendium of Evaluated Constitutional Data and Phase Diagrams," Volume IV, (VCH Publishing New York, NY, 1991).
24. T. KHAN, *Ph.D. Thesis*, University of Cambridge, U.K., 1993.
25. W. F. GALE and J. E. KING, *J. Mater. Sci.* **28** (1993) 4347.
26. R. YANG, J. A. LEAKE and R. W. CAHN, *J. Mater. Res.*, **6**, (1991) 343.
27. W. F. GALE, *Intermetallics*, **4** (1996) 585.
28. W. F. GALE and Z. A. M. ABDO, *J. Mater. Sci.*, Submitted for publication.

Received 25 April
and accepted 21 August 1998